

CALCULATION OF THREE-DIMENSIONAL UNSTEADY SHEET CAVITATION BY A SIMPLE SURFACE PANEL METHOD “SQCM”

Jun Ando and Kuniharu Nakatake
Kyushu University, Fukuoka 812-8581, JAPAN

Abstract

This paper presents a calculation method for the 3-D unsteady cavitating hydrofoil problem. The method is based on a simple surface panel method “SQCM” which satisfies easily the Kutta condition even in the unsteady problem. This method is applied to the Wagner problem, heaving hydrofoil and the hydrofoil in sinusoidal gust. We show some calculated results for partially cavitating and supercavitating hydrofoil and compare them with other calculated results.

1 Introduction

In the fluid machinery such as marine propeller operating at high speed, we can not prevent the occurrence of cavitation. Cavity on the propeller blade produces the pressure fluctuation on the stern hull surface which is one of the causes of the ship vibration and also reduces the propeller performance. Therefore it is important to predict the unsteady cavity pattern and volume etc. accurately, because the unsteadiness of the cavity affects the pressure fluctuation on the stern hull surface. In this paper we treat the unsteady sheet cavitation.

Panel methods, which can represent the blade shape accurately, are recently widely used for the cavitation prediction. The calculated results of unsteady cavitation have been presented by Kim and Lee (1993) and Ando et al. (2000) for 2-D problems, Kinnas and Fine (1992) and Kim et al. (1994) for 3-D problems.

Recently we developed a simple surface panel method “SQCM” which satisfies easily the Kutta condition even in the unsteady problem. In this paper we extend SQCM to the 3-D unsteady sheet cavitating hydrofoil problem and present the calculation method to treat the partially cavitating and supercavitating cases by using the same numerical procedure.

2 Calculation method

2.1 Outline of unsteady SQCM

SQCM (Source and QCM) is a simple surface panel method which is a kind of singularity method. This method uses source distributions (Hess and Smith, 1964) on the hydrofoil surface and discrete vortex distributions arranged on the mean camber surface according to QCM (Quasi-Continuous vortex lattice Method) (Lan, 1974). These singularities should satisfy the boundary condition that the normal velocity is zero on the hydrofoil and the mean camber surfaces.

Let us consider a hydrofoil of chord length c advancing with a constant speed U and doing slow oscillation (see Figure 1). The hydrofoil coordinate system $o - xyz$ and the space coordinate system $O - XYZ$ are introduced as Figure 1. The angle α between the x -axis and the X -axis is defined as the angle of attack of the hydrofoil.

The hydrofoil surface S is divided into M panels in the spanwise direction. The face and back sides of the hydrofoil section are divided into N_m panels in the chordwise direction, respectively. Therefore the total number

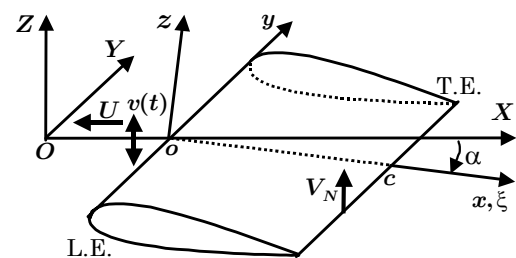


Figure 1: Coordinate systems

of source panels for the hydrofoil surface becomes $M \times 2N_m$ and constant source m in each panel is distributed.

Next the mean camber surface is divided into M segments in the spanwise direction (μ) corresponding to the division of the source panels and divided into N_γ in the chordwise direction. The positions of the bound vortex $\xi_{\mu\nu}^{LP}$ and control point $\xi_{\mu\nu}^{CP}$ on the mean camber surface are expressed by the following equations according to the QCM theory.

$$\xi_{\mu\nu}^{LP} = c_\mu \left[1 - \cos\left\{ (2\nu - 1)\pi / (2N_\gamma) \right\} \right] / 2, \quad \xi_{\mu\nu}^{CP} = \bar{c}_\mu \left\{ 1 - \cos(\nu\pi / N_\gamma) \right\} / 2 \quad (1)$$

Here c_μ is the chord length of the μ -th hydrofoil section, and \bar{c}_μ is the averaged chord length between the μ -th and $\mu + 1$ -th hydrofoil sections.

And total $M \times N_\gamma$ ring vortices are located on the mean camber surface according to Eq. (1). One set of ring vortices consists of one bound vortex, two free vortices and the first spanwise shed vortex closest to the trailing edge(T.E.) in the trailing wake. In case of the unsteady problem the shed vortex flows out from T.E.. Thus the ring vortex which represents the shed vortex is located in the trailing wake. This ring vortex consists of two spanwise shed vortices and two chordwise trailing vortices. Then the shed vortices are assumed to shift on the x -axis by velocity U retaining each strength during one time step.

Summing up the inflow velocity vector \vec{V}_I , the velocity vector due to the source panels \vec{V}_m and the velocity vector due to the vortices \vec{V}_γ , the velocity vector around the hydrofoil in the hydrofoil fixed coordinate \vec{V} is expressed as

$$\vec{V} = \vec{V}_I + \vec{V}_\gamma + \vec{V}_m \quad (2)$$

The detailed expressions \vec{V}_m and \vec{V}_γ are described in the reference (Ando et al., 1998).

We consider that the velocity normal to the mean camber surface at T.E. V_N is zero as the Kutta condition in the steady SQCM. On the other hand we introduce the normal velocity at T.E. in order to make the pressure difference between the upper and lower surfaces zero in the unsteady case. We choose the control points on the upper and the lower source panels at T.E. as the positions where the Kutta condition is satisfied. Here we define the pressure difference as Δp and indicate the upper and the lower surfaces with subscripts $+$ and $-$, respectively. Defining the perturbation potential and the magnitude of velocity on the upper and lower surfaces as ϕ_+ , ϕ_- and V_+ , V_- , respectively, the Kutta condition in the unsteady SQCM is given by

$$\Delta p = \rho \frac{\partial}{\partial t} (\phi_+ - \phi_-) + \frac{1}{2} \rho (V_+^2 - V_-^2) = 0 \quad (3)$$

The boundary conditions at the control points on the hydrofoil and the mean camber surfaces are that there is no flow across the surfaces. But there exists at T.E. the normal velocity which is introduced to satisfy the Kutta condition as expressed by Eq. (3). Therefore the equations of the boundary conditions are given as follows:

$$\left. \begin{array}{l} \vec{V} \cdot \vec{n} = 0 \quad \text{on hydrofoil and camber surface (except T.E.)} \\ \vec{V} \cdot \vec{n} = V_N \quad \text{at T.E.} \end{array} \right\} \quad (4)$$

where \vec{n} is the normal vector on the hydrofoil and the mean camber surfaces.

The unknown values are the source strengths on the hydrofoil surface, the vortex strengths on the mean camber surface and the normal velocity V_N at T.E.. V_N is expressed by the following equation and determine so as to satisfy the Kutta condition iteratively.

$$V_N^{(n+1)} = \Delta p^{(n)} / (\rho U) + V_N^{(n)} \quad (5)$$

Here n is the number of iteration. The first term in the right hand side in Eq. (5) means the corrector for the value of the previous step $V_N^{(n)}$ which is proportional to the pressure difference $\Delta p^{(n)}$. The iteration is continued until the pressure difference becomes small ($|\Delta C_p (= 2\Delta p / \rho U^2)| \leq 10^{-3}$). Assuming the normal velocity V_N at T.E. at each iterative step, Eq. (4) can be solved as the linear simultaneous equations for singularity distributions.

The unsteady pressure distribution on the hydrofoil is calculated by the unsteady Bernoulli equation expressed as

$$p(t) - p_0 = -\frac{1}{2}\rho\left(|\vec{V}|^2 - |\vec{V}_I|^2\right) - \rho\frac{\partial\phi}{\partial t} \quad (6)$$

where

p_0 = the static pressure in the undisturbed inflow, ρ = the density of the fluid
 ϕ = the perturbation potential in the hydrofoil coordinate system

Here the time derivative term of ϕ in Eq. (6) is obtained numerically by two points upstream difference with respect to time. Before numerical differentiation the perturbation potential ϕ is calculated analytically for source and vortex components, respectively. Then the pressure coefficient is defined by

$$C_p = (p - p_0) / (\frac{1}{2}\rho U^2) \quad (7)$$

The lift L and the drag D of the hydrofoil are defined by the forces in the Z direction and the X direction in the space coordinate system, respectively. The lift and drag coefficients are defined by

$$C_L = L / (\frac{1}{2}\rho A U^2), C_D = D / (\frac{1}{2}\rho A U^2) \quad (8)$$

where A is projected area of the hydrofoil on the xy -plane.

After above calculation, the trailing vortices are shifted backward and the time step t_L is changed into t_{L+1} .

2.2 Calculation method for unsteady cavitation

Denoting the cavitation number and the tangential velocity on the cavity surface S_c by σ and V_T , respectively, we have the following relation in the unsteady problem.

$$V_T = \sqrt{(1 + \sigma)U^2 - 2\partial\phi/\partial t} \quad (9)$$

In the present calculation method we assume first the cavity length ℓ_μ for each spanwise section. Next we give the cavitation number σ in Eq. (9) and obtain the tangential velocity V_T , and then determine the source and vortex distributions from the following equation.

$$(\Phi_{\mu v} - \Phi_{\mu v-1}) / \Delta s_{\mu v} = V_T \{1 - f(s_{f\mu})\} \quad (10)$$

Here $\Phi_{\mu v}$ and $\Phi_{\mu v-1}$ are the total velocity potential on the control points of the v -th and $v-1$ -th cavity surface panels in the chordwise direction, respectively. $\Delta s_{\mu v}$ means the distance between these two control points (See Figure 2). In eq. (10), we adopt the cavity termination model used by Kinnas and Fine (1993), that is,

$$f(s_{f\mu}) = \begin{cases} 0 & , s_{f\mu} < s_{T\mu} \\ A_T \{(s_{f\mu} - s_{T\mu}) / (s_{L\mu} - s_{T\mu})\}^{v_T} & , s_{T\mu} < s_{f\mu} < s_{L\mu} \end{cases} \quad (11)$$

where $s_{f\mu}$ represents the distance from the cavity detachment point along the hydrofoil surface and A_T ($0 < A_T < 1$) and v_T ($v_T > 0$) are proper constants. Eq. (11) means that the tangential velocity changes gradually according to the shape of function $1 - f(s_{f\mu})$ in the transition region between the cavity end point $s_{L\mu}$ and the point $s_{T\mu}$ in front of the point $s_{L\mu}$ and becomes non-zero value $V_T(1 - A_T)$ at $s_{L\mu}$. The length of the transition region is expressed as $\lambda\ell_\mu$. Here λ is also a proper constant. In the present calculation we adopt $A_T = 0.2$, $v_T = 1.0$, $\lambda = 0.1$.

On the other hand the boundary conditions on the hydrofoil surface S except the cavity surface and on the mean camber surface C are that there is no flow across the surfaces. These boundary conditions are the same as those of SQCM expressed by Eq. (4). From Eqs. (4) and (10), we can derive $(2N_m + N_\gamma) \times M$ linear simultaneous equations which determine m , γ . When we calculate the velocity on the cavity surface using these singularity distributions, we can not satisfy the boundary condition on the cavity surface. Therefore we need

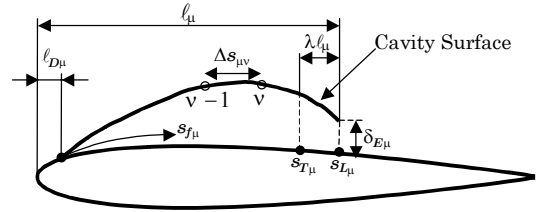


Figure 2: Partially cavitating hydrofoil

rearrange the source panels on the cavity surface so as to coincide with the flow direction calculated by these singularity distributions.

Defining the cavity height of the v -th panel at the present time t_L as $h_{\mu v}(t_L)$, $h_{\mu v}(t_L)$ is expressed by the following equation.

$$h_{\mu v}(t_L) = \left\{ \vec{V}_I \cdot \vec{n} + \frac{\partial \phi}{\partial n} + \frac{\mathbf{V}_T}{\Delta s_{\mu v}} h_{\mu v-1}(t_L) + \frac{h_{\mu v}(t_{L-1})}{\Delta t} \right\} / \left\{ \frac{\mathbf{V}_T}{\Delta s_{\mu v}} + \frac{1}{\Delta t} \right\} \quad (12)$$

We repeat two steps, that is, solving Eqs. (4) and (10) and rearranging the source panels on the cavity surface until the cavity shape converges.

After rearranging the source panels, we adjust the cavity length by using the following equation so that the height of opening $\delta_{\mu}(t_L)$ at the cavity end is close to the target opening $\delta_{E\mu}$.

$$\ell_{\mu}^{(n+1)}(t_L) = \ell_{\mu}^{(n)}(t_L) + w\delta_{\mu}(t_L) \quad (13)$$

Here n and w are the iteration number for adjusting the cavity length and a proper weight coefficient, respectively. Modifying the opening at the cavity end proposed by Ito (1986), we adopt the following equation for $\delta_{E\mu}$.

$$\delta_{E\mu} = 0.8\alpha^2 \ell_{\mu}(t_L) \quad (14)$$

We repeat the calculation described above until the following condition is satisfied.

$$|\delta_{\mu}(t_L) - \delta_{E\mu}| \leq c_{\mu} \times 10^{-3} \quad (15)$$

When the calculated opening at the cavity end $\delta_{\mu}(t_L)$ satisfies Eq. (15), we move to the next time t_{L+1} .

If the cavity length $\ell_{\mu}(t_L)$ is in the following range, we enforce that $\ell_{\mu}(t_L)$ equals to ℓ_{\max} .

$$\ell_{\min}(= 0.99c_{\mu}) \leq \ell_{\mu}(t_L) \leq \ell_{\max}(= 1.05c_{\mu}) \quad (16)$$

This is because it is difficult to converge the cavity shape when the cavity length nearly equals to the chord length. The calculation method in the supercavitating case is basically the same as that in the partially cavitating case. However we only use Eq. (4) as the boundary condition for the spanwise section which contains both the partially cavitating and supercavitating cases. At that section the cavity shape is determined by interpolation using the cavity shapes at the neighboring sections. We adopt the following equation for the opening at the cavity end for all cavity length in the supercavitating case.

$$\delta_{E\mu} = 0.8\alpha^2 \quad (17)$$

3 Calculated results

In the present calculation, we take 640 panels ($2N_m = 40, N = 16$) on the hydrofoil surface and do 336 bound vortices ($N_{\gamma} = 21, N = 16$) on the mean camber surface. We assume that the location of the cavity detachment point is 0.6% chord length from the leading edge.

As the first example, we calculate about the rectangular hydrofoil of aspect ratio, $AR=2.778$, advancing with constant speed U abruptly from rest state at $\alpha = 6^\circ$ (Wagner problem). The hydrofoil has NACA16-206 section at all spanwise positions and we take the time increment $dt = 0.1c/U$.

Figure 3 shows the cavity planform variation comparing with the experimental data (Ukon, 1986) and the calculated result (Ando et al., 1999) in the steady condition. We can see that the cavity grows with time and finally approaches both the experimental and calculated results in the steady condition.

Next we show the calculated results for the rectangular hydrofoil of aspect ratio, $AR=5.0$, in heaving motion of the vertical displacement $h = h_0 e^{i\omega t}$, where $h_0(= 0.01c)$ is the amplitude of heaving and ω is the circular frequency. The hydrofoil has NACA0006 section at the midspan, tapering elliptically to zero at the tip of the

hydrofoil, and is set at $\alpha = 5^\circ$. Defining the reduce frequency, $k = \omega c / 2U = 0.5$, and cavitation number, $\sigma = 0.2$, we compare our calculated results with Kim et al.'s ones (1994). In this calculation, we take the time increment $dt = \pi c / 10kU$. In order to reduce the computing time we start the calculation of Wagner problem to approach the steady condition. Then we begin the unsteady calculation.

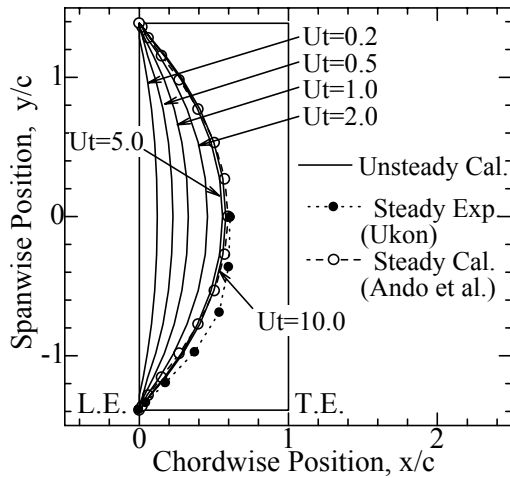


Figure 3: Cavity planform variation versus time on Wagner problem (Rectangular hydrofoil, NACA16-206, AR=2.778, $\alpha = 6^\circ$, $\sigma = 0.628$, $dt = 0.1c/U$)

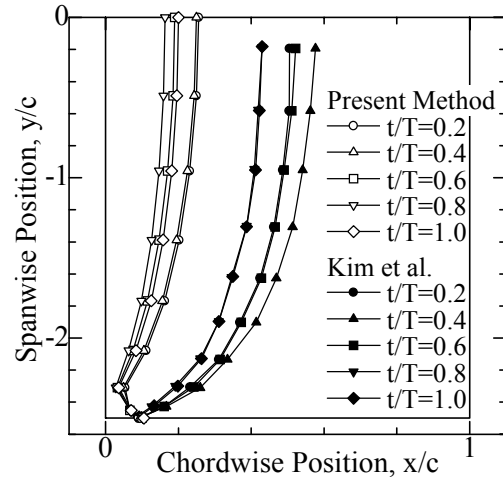


Figure 4: Cavity planform variation versus time in heave (Rectangular hydrofoil, NACA0006, AR=5.0, $\alpha = 5^\circ$, $\sigma = 1.2$, $h_0 = 0.01c$, $k = 0.5$, $dt = \pi c / 10kU$)

Figure 4 shows the cavity planform variation in one cycle. Both the cavity length and the width of variation in the present method are smaller than Kim et al.'s ones. These discrepancies may be caused by the difference of the treatment of the tangential velocity on the cavity surface and the cavity detachment point.

Figure 5 and 6 shows the lift and drag coefficient variations with respect to time. Discrepancies between the present results and Kim et al.'s results are observed because Kim et al. did not considered the unsteady pressure term, $-\rho \partial \phi / \partial t$, in the pressure calculation for the first two cycles. After the third cycle both calculated results agree with each other.

Next we show the calculated results for the rectangular hydrofoil of aspect ratio, AR=2.778, advancing in the sinusoidal gust whose vertical speed $v(x,t)$ is $v_0 e^{i\nu(t-x/U)}$, where $\nu = 2\pi U / \lambda$, λ is the wave length of the gust and $v_0 (= 0.02U)$ is the gust amplitude. In this case, the reduced frequency k is given by $\pi c / \lambda$. The hydrofoil has NACA16-206 at all spanwise sections and is set at $\alpha = 6^\circ$.

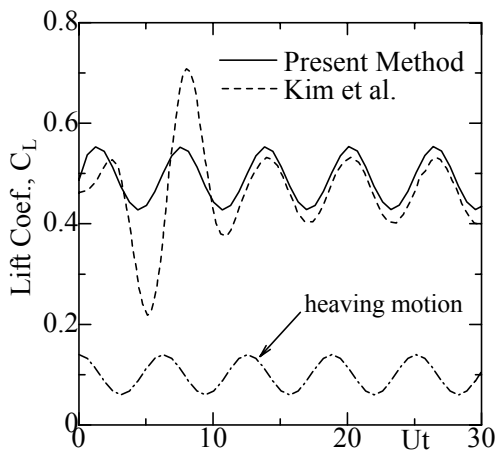


Figure 5: Lift coefficient variation versus time in heave (Rectangular hydrofoil, NACA0006, AR=5.0, $\alpha = 5^\circ$, $\sigma = 1.2$, $h_0 = 0.01c$, $k = 0.5$, $dt = \pi c / 10kU$)

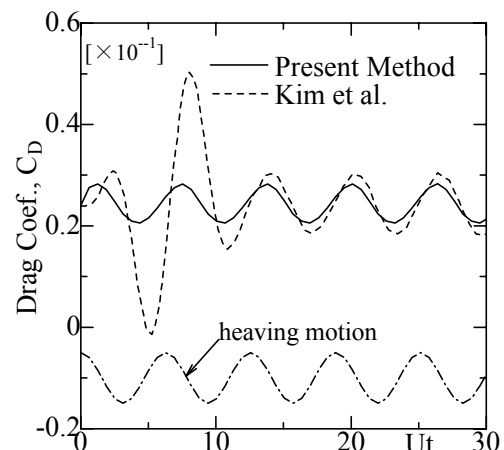


Figure 6: Drag coefficient variation versus time in heave (Rectangular hydrofoil, NACA 0006, AR=5.0, $\alpha = 5^\circ$, $\sigma = 1.2$, $h_0 = 0.01c$, $k = 0.5$, $dt = \pi c / 10kU$)

Figure 7 shows the cavity planform variation in one cycle for the conditions of $\sigma = 0.628$, $k = 0.5$, $dt = \pi c / 20kU$. We can see that the cavity planform varies smoothly in wide range.

Figure 8 shows the variations of cavity length, ℓ/c , and cavity volume, $Vol./c^3$, at midspan and Figure 9 does the lift and drag coefficient variations with respect to time. The variations of the vertical component of inflow at the leading edge of the hydrofoil are also shown in these figures. The phases of these results lag behind the heaving motion.

Figure 10 shows the cavity shape variation and Figure 11 does the pressure distribution variation at midspan with respect to time. The pressure coefficient, $C_p (= -\sigma)$, at the back side becomes constant corresponding to the target cavitation number.

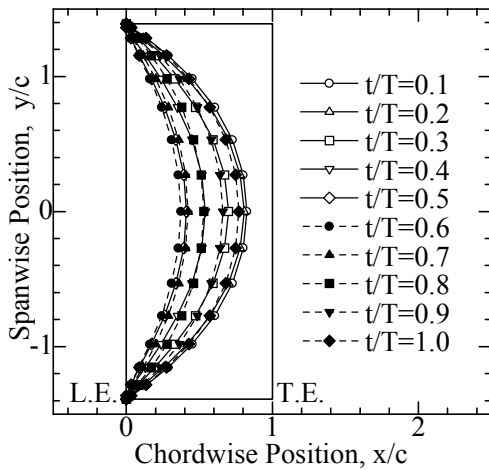


Figure 7: Cavity planform variation versus time in sinusoidal gust (Rectangular hydrofoil, NACA16-206, $AR=2.778$, $\alpha=6^\circ$, $\sigma = 0.628$, $v_0=0.02U$, $k=0.5$, $dt=\pi c / 20kU$)

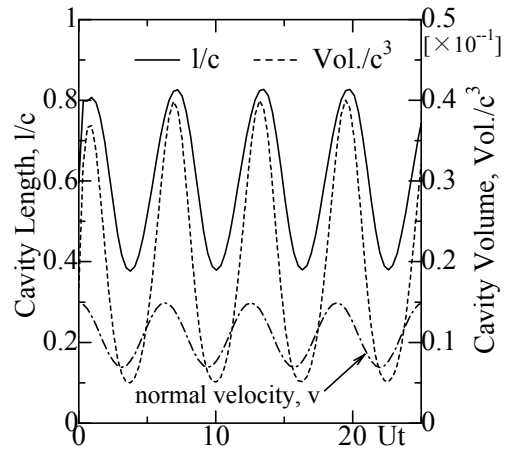


Figure 8: Cavity length variation at midspan and cavity volume variation versus time in sinusoidal gust (Rectangular hydrofoil, NACA16-206, $AR=2.778$, $\alpha=6^\circ$, $\sigma = 0.628$, $v_0 = 0.02U$, $k = 0.5$, $dt = \pi c / 20kU$)

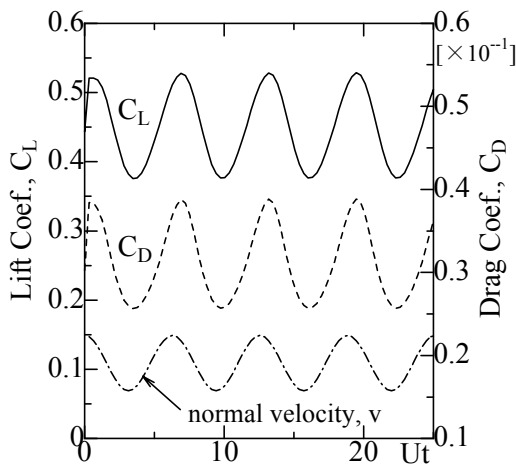


Figure 9: Lift and drag coefficients versus time in sinusoidal gust (Rectangular, hydrofoil, NACA16-206, $AR=2.778$, $\alpha=6^\circ$, $\sigma = 0.628$, $v_0=0.02U$, $k=0.5$, $dt=\pi c / 20kU$)

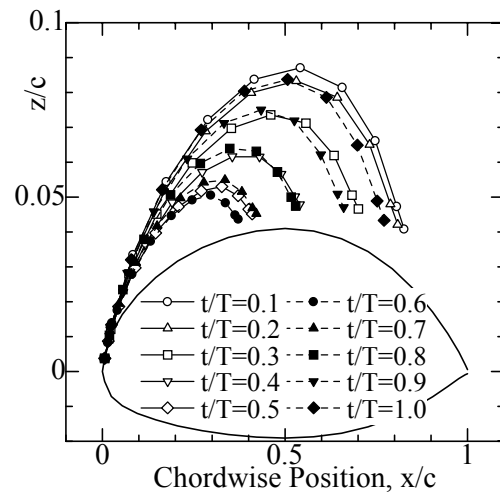


Figure 10: Cavity shape variation at midspan versus time in sinusoidal gust (Rectangular hydrofoil, NACA16-206, $AR=2.778$, $\alpha=6^\circ$, $\sigma=0.628$, $v_0=0.02U$, $k=0.5$, $dt = \pi c / 20kU$)

Finally we show the results at $\sigma = 0.2$ for the just above-mentioned hydrofoil in the same sinusoidal gust. Here we take the time increment $dt = \pi c / 10kU$. Both of the partially cavitating and supercavitating cases exist in this calculation.

Figure 12 shows the cavity planform variation in one cycle. The cavity planform varies continuously holding partially cavitating region near the tip of the hydrofoil and supercavitating region around midspan.

Figure 13 shows the variations of cavity length and cavity volume at midspan and Figure 14 does the lift and drag coefficient variations with respect to time. These results, especially the lift and drag coefficients, do not vary smoothly. The unstable partially cavitating region near the tip of the hydrofoil may cause these inaccurate results.

Figure 15 shows the cavity shape variation and Figure 16 does the pressure distribution variation at midspan with respect to time. The pressure coefficient at the back side becomes almost constant in the supercavitating case too.

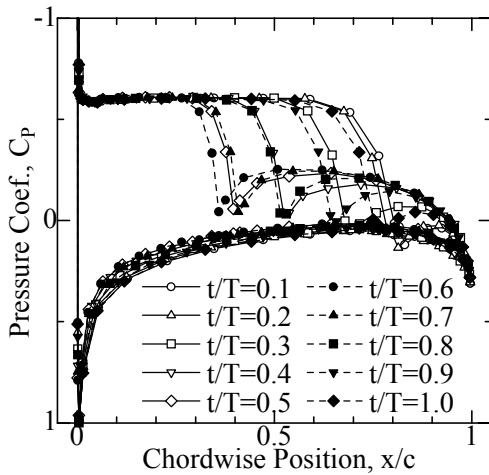


Figure 11: Pressure distribution variation at midspan versus time in sinusoidal gust (Rectangular hydrofoil, NACA16-206, AR=2.778, $\alpha = 6^\circ$, $\sigma = 0.628$, $v_0 = 0.02U$, $k = 0.5$, $dt = \pi c / 20kU$)

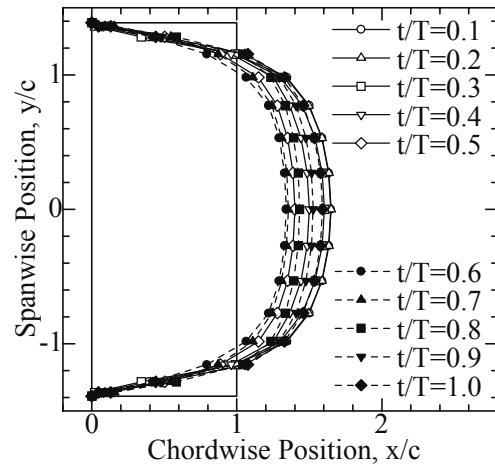


Figure 12: Cavity planform variation versus time in sinusoidal gust (Rectangular hydrofoil, NACA 16-206, AR=2.778, $\alpha = 6^\circ$, $\sigma = 0.2$, $v_0 = 0.02U$, $k = 0.5$, $dt = \pi c / 10kU$)

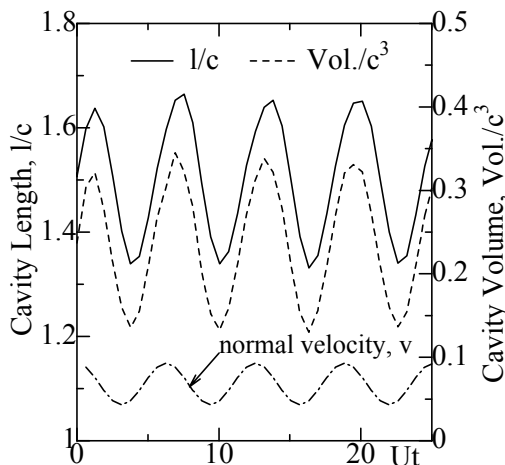


Figure 13: Cavity length variation at midspan and cavity volume variation versus time in sinusoidal gust (Rectangular hydrofoil, NACA16-206, AR=2.778, $\alpha = 6^\circ$, $\sigma = 0.2$, $v_0 = 0.02U$, $k = 0.5$, $dt = \pi c / 10kU$)

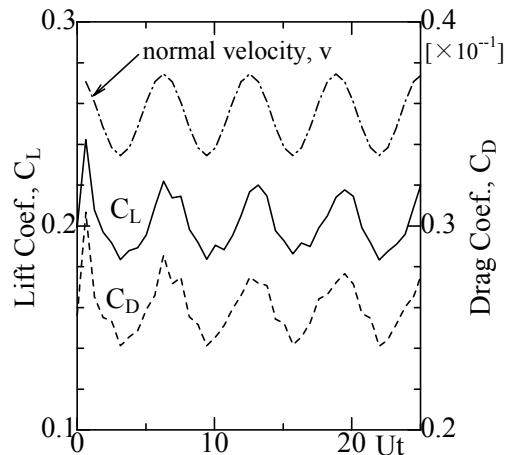


Figure 14: Lift and drag coefficients versus time in sinusoidal gust (Rectangular hydrofoil, NACA 16-206, AR=2.778, $\alpha = 6^\circ$, $\sigma = 0.2$, $v_0 = 0.02U$, $k = 0.5$, $dt = \pi c / 10kU$)

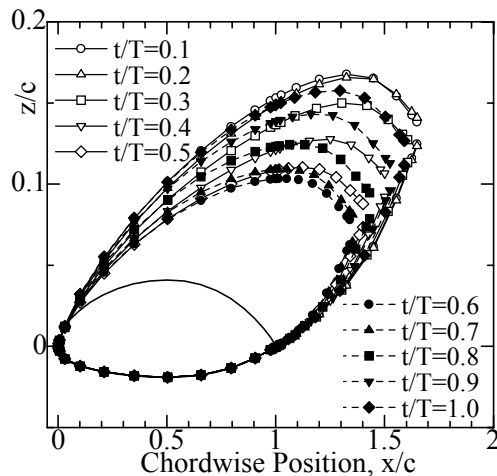


Figure 15: Cavity shape variation at midspan versus time in sinusoidal gust (Rectangular hydrofoil, NACA16-206, AR=2.778, $\alpha=6^\circ$, $\sigma=0.2$, $v_0=0.02U$, $k=0.5$, $dt=\pi c/10kU$)

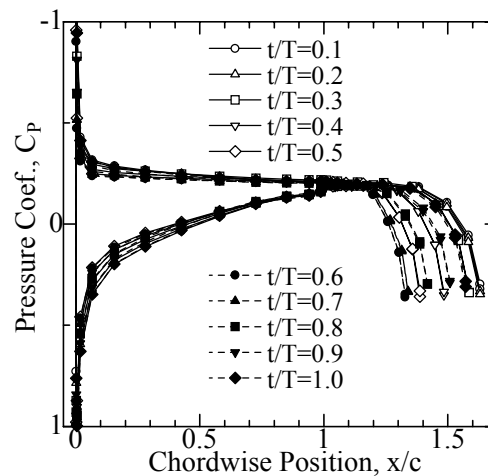


Figure 16: Pressure distribution variation at midspan versus time in sinusoidal gust (Rectangular hydrofoil, NACA16-206, AR=2.778, $\alpha=6^\circ$, $\sigma=0.2$, $v_0=0.02U$, $k=0.5$, $dt=\pi c/10kU$)

4 Conclusions

In this paper we presented a calculation method for the 3-D unsteady sheet cavitating hydrofoil problem by applying a simple surface panel method "SQCM". We treated the partially cavitating hydrofoil in heaving motion and both partially cavitating and supercavitating hydrofoil in sinusoidal gust. Calculated results are compared with other calculated results and the accuracy of the present results is confirmed. The present method will be extended to the unsteady cavitating propeller problem.

References

- Ando, J., Maita, S. and Nakatake, K., 1998, "A New Surface Panel Method to Predict Steady and Unsteady Characteristics of Marine Propeller", *Proc. of the 22nd Sympo. on Naval Hydrodynamics*, pp.142-155
- Ando, J., Matsumoto, D., Maita, S., Ohashi, K. and Nakatake, K., 1999, "Calculation of Three-Dimensional Steady Cavitation by a Simple Surface Panel Method", *J. of the Soc. of Naval Architects of Japan*, **Vol. 186**, pp.17-27 (in Japanese)
- Ando, J. Shirao, A., Kanemaru T., Ohashi, K. and Nakatake, K., 2000, "Calculation of 2-D Unsteady Sheet Cavitation by a Simple Surface Panel Method", *Trans. of the West-Japan Soc. of Naval Architects*, **No. 100**, pp.157-169 (in Japanese)
- Hess, J.L. and Smith, A.M.O., 1964, "Calculation of Nonlifting Potential Flow about Arbitrary Three Dimensional Bodies", *J. of Ship Research*, **Vol. 8, No. 2**, pp.22-44
- Ito, J., 1986, "Calculation of Partially Cavitating Thick Hydrofoil and Examination of a Flow Model at Cavity Termination", *Proc. of Int. Sympo. on Cavitation*, **Vol. 1**, pp.209-214
- Kim, Y.-G. and Lee, C.-S., 1993, "Prediction of Unsteady Cavity Behavior around a 2-D Hydrofoil in Heave or Gust", *Proc. of the 2nd Japan-Korea Joint Workshop on Ship and Marine Hydrodynamics*, pp.299-308
- Kim, Y.-G., Lee, C.-S. and Suh, J.-C., 1994, "Surface Panel Method for Prediction of Flow around 3-D Steady or Unsteady Cavitating Hydrofoil", *Proc. of the 2nd Int. Sympo. on Cavitation*, pp.113-120
- Kinnas, S.A. and Fine, N.E., 1992, "A Nonlinear Boundary Element Method for the Analysis of Unsteady Propeller Sheet Cavitation", *Proc. of the 19th Sympo. on Naval Hydrodynamics*, pp.717-737
- Kinnas, S.A. and Fine, N.E., 1993, "A Numerical Nonlinear Analysis of the Flow around Two- and Three-Dimensional Partially Cavitating Hydrofoils" *J. of Fluid Mechanics*, **Vol. 254**, pp.151-181
- Lan, C.E., 1974, "A Quasi-Vortex-Lattice Method in Thin Wing Theory", *J. of Aircraft*, Vol. 11, No. 9, pp.518-527
- Ukon, Y., 1986, "Cavitation Characteristics of a Finite Swept Wing and Cavitation Noise Reduction due to Air Injection", *Proc. of Int. Sympo. on Propeller and Cavitation*, pp.383-390